PNAS
www.pnas.org

Supplementary Information for:

Activin-A limits Th17 pathogenicity and autoimmune neuroinflammation via CD39 and CD73 ectonucleotidases and Hif1-α -dependent pathways.

Ioannis Morianos[1], Aikaterini I. Trochoutsou[1#], Gina Papadopoulou[1#], Maria Semitekolou[1], Aggelos Banos[2], Dimitris Konstantopoulos[3], Antigoni Manousopoulou[4], Maria Kapasa[5], Ping Wei[6], Brett Lomenick[7], Elise Belaidi[8,9], Themis Kalamatas[10], Klinta Karageorgiou[11], Triantafyllos Doskas[12], Federica Sallusto[13], Fan Pan[6], Spiros D. Garbis[7#], Francisco J. Quintana[14#] and Georgina Xanthou[1*]

[1]Cellular Immunology Laboratory, Biomedical Research Foundation of the Academy of Athens (BRFAA) Athens, 11527, Greece; [2]Division of Immunobiology, BRFAA, Athens, 11527, Greece; [3]Department of Molecular Biology and Genetics, Biomedical Sciences Research Center 'Alexander Fleming', Athens, 16672, Greece; [4]Beckman Research Institute, City of Hope National Medical Center, Duarte, CA, 91010, USA; [5]Molecular Biology Laboratory, BRFAA, Athens, 11527, Greece; [6]Department of Oncology and Medicine, Sidney Kimmel Comprehensive Cancer Center, Johns Hopkins University School of Medicine, Maryland 21231, USA; [7]Proteome Exploration Laboratory, Beckman Institute, Division of Biology and Biological Engineering, California Institute of Technology, Pasadena, CA, 91125, USA; [8]Laboratoire HP2, University of Grenoble Alpes, HP2, Grenoble F-38042, France; [9]INSERM Grenoble U1042, France; [10]Department of Neurology, 'G. Gennimatas' General State Hospital of Athens, 11527, Greece; [11]Department of Neurology, Athens Medical Center, Athens, 15125, Greece; [12]Department of Neurology, Athens Naval Hospital, Athens, 11521, Greece; [13]Institute of Microbiology, ETH, Zürich, 8093, Switzerland; [14]Ann Romney Center for Neurologic Diseases, Brigham and Women's Hospital, Harvard Medical School, Boston/The Broad Institute of MIT and Harvard, Boston, MA, 02115, USA.

[#]Equal contribution

*Corresponding author:
Georgina Xanthou, PhD
Cellular Immunology Laboratory,
Biomedical Research Foundation of the Academy of Athens,
Athens 115 27 Greece
Tel: +30-210-6597 336
Email: gxanthou@bioacademy.gr

This PDF file includes:

Supplementary information text
Figures S1 to S8
Tables S1 to S2
SI References

Supplementary Information Text

SI Materials and Methods

Human Subjects

Serum, CSF and peripheral blood were obtained from patients with RMMS (*n*=23), according to the McDonald's revised diagnostic criteria (1), age-matched disease controls (patients with no evidence of autoimmune disease, *n*=20) and healthy controls (*n*= 10). The age range of the RMMS patients was 24-66 years. On entering the study, subjects were in a stable condition and did not develop any clinical signs of infection for at least 4 weeks before evaluation. Information on all donors is given in Table S1. Human participants signed an informed consent form and the study protocol was approved by the Scientific Research Ethics Committees of 'G. Gennimatas' General State Hospital of Athens and the Athens Naval Hospital.

Mice

8-12 week-old female mice were maintained at the BRFAA, the Johns Hopkins Animal Facility and the animal facility of the University of Grenoble. C57BL/6, C57BL/6-*Rag1*$^{-/-}$, C57BL/6-*Nt5e*$^{-/-}$ (B6.129S1-Nt5etm1Lft/J), *Cd4*Cre (Tg(Cd4-cre)1Cwi) and LSL-Hif1dPA (B6.129S6(C)-Gt(ROSA)26Sortm3(Hif1A*) Kael/J) (2) mice were purchased from the Jackson Laboratory. Phd1 (*Egln*2)$^{-/-}$ mice were generated in Peter Carmeliet's group (VIB, Leuven, Belgium), as previously described (3) and breeding couples were provided for colony expansion at the animal facility of the University of Grenoble. *Il17a*^{Cre} and *Il17a*^{Cre}/*R26R*^{eYFP} mice on the C57BL/6 background were kindly provided by Prof. Brigitta Stockinger (4). *R26R*^{eYFP} mice on the C57BL/6 background were kindly provided by Prof. Frank Costantini (5). 2D2 TCR transgenic mice were kindly provided by Prof. Lesley Probert (Hellenic Pasteur Institute, Athens, Greece). Mice from different experimental groups,

including knockout and their WT counterparts, were housed in the same cage to limit the impact of inter-individual microbiota on the variability of the experimental outcome. Animal handling and procedures were in accordance with US National Institutes of Health Statement of Compliance (Assurance) with Standards for Humane Care and Use of Laboratory Animals (#A5736-01 and A38 516 10006), in compliance with the Johns Hopkins Animal Care and Use Policies, and with the European Union Directive 86/609/EEC on protection of animals used for experimental purposes.

Isolation and culture of human CD4$^+$ T cells

Peripheral blood mononuclear cells (PBMCs) were obtained from RRMS patients and healthy age-matched controls by Histopaque (Sigma Aldrich) density-gradient centrifugation. Naive CD4$^+$ T cells (Miltenyi Biotec) and total CD4$^+$ T cells (Dynal CD4 positive isolation kit, Invitrogen) were isolated. Naive CD4$^+$ T cells were differentiated towards Th17 cells with plate-bound anti-CD3 (2μg/ml; OKT3; Biolegend) and soluble anti-CD28 (2μg/ml; CD28.2; Biolegend) in 96-well plates, supplementated with recombinant IL-6 (Peprotech, 50ng/ml), IL-1β (Peprotech, 20ng/ml) and IL-23 (Peprotech, 20ng/ml) in the presence of PBS (control) or activin-A (100ng/ml, R&D Systems) for 7-10 days. CD4$^+$ T cells ($5x10^4$) were activated with plate-bound anti-human CD3 and soluble anti-human CD28 (as above) in the presence of PBS or recombinant activin-A (100ng/ml, R&D Systems) for 3-5 days 7 (6). Dose-response studies determined the optimal doses of activin-A and anti-CD3/CD28 antibodies. Gene expression was analyzed by quantitative PCR, cytokine levels were evaluated by ELISA in culture supernatants and by flow cytometry following intracellular staining.

Induction of active EAE and scoring

EAE was induced as described (7). Briefly, C57BL/6 mice were immunized subcutaneously, on day 0 with an 1:1 emulsion of 200 mg myelin oligodendrocyte glycoprotein peptide (MOG_{35-55}) (GENEMED Synthesis) in complete Freund's adjuvant (CFA) (Sigma-Aldrich), containing 4 mg/ml heat-killed *Mycobacterium tuberculosis* H37Ra (Difco Laboratories). 300ng *Bordetella pertussis* toxin (PTX) (List Biological Laboratories) diluted in PBS, was given intraperitoneal (i.p.) at the time of immunization (day 0) and on day 2. Clinical signs of EAE were assessed (7). Incorporated radioactivity was counted using a β-scintillation counter (Microbeta-Trilux; PerkinElmer). Cytokine release was measured in culture supernatants by ELISA.

Characterization of CNS immune cells in mice

Spinal cords were dissected at the peak of EAE (days 17-20) and treated with the collagenase D cocktail (Millipore) (2.5mg/ml) for 1h at 37^{o}C (7). Tissues were homogenized through a 70mm cell strainer (BD Biosciences) and mononuclear cells were isolated by a 30-70% Percoll (Sigma-Aldrich) gradient centrifugation. Residual red blood cells were lysed by hypotonic solution. Immune cells were washed with PBS, labeled with fluorescently-conjugated antibodies and analyzed by flow cytometry.

Quantification of inflammatory foci in CNS tissue

Spinal cords were fixed in 10% (v/v) saline-buffered formalin and embedded in paraffin. Four-micrometer sections were stained with hematoxylin and eosin (H&E) to evaluate spinal cord inflammation (7). For axonal demyelination evaluation, dehydrated sections were incubated overnight at 57^{0}C with a solution of Luxol Fast Blue (LFB) (Sigma Aldrich), washed, rinsed in 0.05% lithium carbonate and stained in a solution of Cresyl Violet (Sigma Aldrich) for 6 min, at 57^{0}C. Sections were

washed, dehydrated and prepared for microscope analysis. Analyses of all histology and microscopy data were performed blindly by two independent observers.

Free ATP measurement assay

Act-A-Th17 or Th17 cells were differentiated as described in the main Materials and Methods section, for 48h. Cells were washed twice with phenol red-free RPMI 1640 (Gibco, USA) and serum-starved overnight. ATP (500μM; Jena Bioscience) was added in the last 8h of culture. ATP concentration was measured in culture supernatants using the ATPlite Luminescence Assay System (PerkinElmer).

Immunofluorescence microscopy

T cell cytospins ($5x10^4$ cells/slide) were prepared in poly-L-lysine slides (Thermo Scientific), fixed in 4% paraformaldehyde (at 4^oC) and incubated in 10% sucrose (6). Slides were washed twice with PBS and blocked in 10% donkey serum, diluted in 0.1% Triton-X. Slides were incubated overnight at 4^oC with primary antibodies against mouse AhR (Santa Cruz), c-Maf (Santa Cruz) and Hif1-α (R&D Systems) or isotype controls (R&D Systems). Slides were washed and incubated with fluorescently-labeled secondary antibodies (Invitrogen) for 1h, RT. Nuclear staining and mounting were carried out using To-pro-3 (ThermoFischer Scientific T3605) and Fluoromount-G (eBioscience 00-4958). Image acquisition was performed using a confocal laser scanning microscope (Leica TCS SP5) and differential interference contrast optics. Immunofluorescence data analysis was performed with the Image J software. AhR $^+$, c-Maf$^+$ and Hif1-α$^+$ T cells were counted in each cytospin by two independent observers in a blinded fashion and expressed as the percentages of total $CD4^+$ T cells (6).

Flow-cytometry analysis

Cells were stained with fluorescently-labeled antibodies against CD45, CD11b, Ly6C, CD4, CD73, CD39, CD3, CD8, and CD25 (all from eBioscience) and TCR γ/δ (Biolegend). For intracellular cytokine staining, cells were stimulated for 4h at 37^0C in medium containing PMA (10 ng/ml, Sigma), ionomycin (250 ng/ml, Sigma-Aldrich) and Golgi-Stop (1μl/ml, BD Biosciences) (6,8). Cells were stained with antibodies against IL-17 (eBioscience and Biolegend), IFN-γ, GM-CSF, IL-10 and Foxp3, phospho-STAT3 (Tyr705) (BD Biosciences), according to the manufacturer's instructions. FACS acquisition was performed with the cytometer Cytomics FC500 (Beckman Coulter) and a BD FACSAria II (Becton Dickinson). Flow cytometry data were analyzed using the FlowJo software 8.7 (Tree Star, Inc).

Quantitative real-time PCR analysis

Total RNA was isolated using the RNAeasy Mini Kit (Qiagen) and reverse-transcribed using Superscript II (Invitrogen), according to the manufacturer's recommendations. The same amount of RNA was used in each cDNA synthesis reaction measured by NanoDrop Spectrophotometer (ThermoScientific). Gene expression was analyzed using SYBR Green Master mix and selected primers (Table S2).-add human primer sets. The relative gene expression over the expression of *Gapdh* and *Polr2a* was calculated using the 2-ΔΔCt analysis method (9).

Immunoblot analysis

Act-A-Th17 or Th17 cells were washed with PBS and harvested in lysis buffer supplemented with protease and phosphatase inhibitors (Invitrogen) (6). Protein homogenates were quantified using the Bradford assay (Thermo Scientific) and 5μg protein was loaded on an acrylamide gel (Biorad). The gel

was transferred onto a PVDF membrane (Millipore), blocked with 5% non-fat milk at 25^{o}C for 1h, and probed with primary antibodies against AhR (Enzo; BML-SA210), c-Maf (Santa Cruz; sc-7866), Hif1-α (R&D; AF1935) and TATA-binding protein (TBP) (Santa Cruz; SC-204), at 4^{o}C overnight. The blot was subsequently incubated with horseradish peroxidase-linked secondary antibodies at 25^{o}C for 1h, and developed using the ECL Chemiluminescence kit (Millipore). Protein expression was normalized by dividing the densitometric units corresponding to the protein of interest with that of TBP from the same sample.

For the cycloheximide chase assay, on the 3rd day of Th17 differentiation, cycloheximide was added in the cultures (100μg/ml; Calbiochem) for 8 hours. Cycloheximide- and control-treated Th17 and act-A-Th17 cells were harvested as above and the protein levels of Hif1-α were quantitated via western blot analysis.

Cytokine analysis

Cytokines were measured in mouse CNS homogenates and cell culture supernatants, in human CSF and serum samples and in human T cell culture supernatants (6,8,10) using commercially available ELISA kits for activin-A, IL-17, IL-1β, IFN-γ, IL-10, TNF-α and GM-CSF (R&D Systems). For ELISA analysis a 4-parameter logistic (4-PL) curve-fit was used for ELISA analyses following the manufacturer's recommendations (R&D Systems).

Chromatin immunoprecipitation

Act-A-Th17 or Th17 cells (8x10^{6} per condition) were fixed for 10 min with 1% formaldehyde at RT and quenched with 0.125M glycine (6,10). Chromatin was prepared by cell lysis and fragmentation was performed by Covaris sonication. Chromatin fragments were incubated overnight at 4°C with anti-

mouse AhR (Enzo BML-SA210), c-Maf (Santa Cruz sc-7866) and STAT3 (Cell Signaling 79D7) or control host-matched IgG antibodies. The immunocomplexes were isolated using magnetic beads (Dynabeads Protein G, Life Technologies). DNA was extracted from immunoprecipitated complexes by reverse crosslinking at 65°C and proteinase K treatment. DNA fragments were purified using NGS magnetic beads (Macherey-Nagel 744970). The relative enrichment of ChIP versus IgG (relative to input DNA) precipitated DNA was determined by qPCR analysis for the regions of interest, using the following primer pairs:

NT5e Site 1: FW: 5'- CGGCTCCCAACAGCACTTGT - 3', REV: 5' - TGCCCTCCCCTTCAGCTTCT – 3' (-3kb); *NT5e* Site 2: FW: 5' – AGCAAGAGAAATAGCAGGGCG – 3', REV: 5' – GTTAGAGCCGTTCTTGCATTGAG - 3'; *Entpd1* Site 1: FW: 5' – CTTACACCGTCCTCCCTGAG – 3', REV: 5'- GCCAGCTGTGAAATGACAAA – 3'; *Entpd1* Site 2: FW: 5' – AAGGAGGTGGACACAACCAG – 3', REV: 5' – TGAATAAATGTGTGCAGAAGGA – 3'; *Entpd1* STAT3-SRE1: FW: 5'-GCTGGGCTTTAGAGACTTGTGGGC -3', REV: 5'-ACCCATGCAAATGGTTTGGGCA-3'; *Il10* : AhR -300bp: FW: 5' – ACCTGGGAGTGCGTGAATGGAATCC – 3', REV: 5' – GTGACTTCCGAGTCAGCAAGAAATA – 3'; *Il10*: c-Maf MARE1: FW: 5' – GGAGAAAGTGAAAGGGATGGAG – 3', REV: 5' – GGAATGGAATTGACTCAAGAACTG – 3'; *Il10*: c-Maf MARE2: FW: 5' – ACCCTCTACATGGGTCTACTT – 3', REV: 5' – CAAGCAACTACTTGTCCTCCT – 3' ; *Cyp1a1*: FW: 5'-AGGCTCTTCTCACGCAACTC- 3', REV: 5'- CTGGGGCTACAAAGGGTGAT- 3'; *Egln2* XRE2: FW: 5'- TAGATGACAGACTGGGCCAC-3', REV: 5'-TGTCTCCCTATCACCTTCCTC-3'.

Sequential chromatin immunoprecipitation

To identify putative STAT3 and AhR co-binding sites, called peaks from ChIP-seq SRA datasets (11) were intersected using bedtools, and overlapping regions were further examined for enriched STAT3 and AhR DNA motifs, using JASPAR motif database. Act-A-Th17 or Th17 cells ($12x10^6$ per condition) were treated as above. After chromatin fragmentation, immunoprecipitation was performed overnight at 4°C using anti-STAT3 antibody (Cell Signaling 79D7) or control rabbit IgG antibody. The immunocomplexes were isolated using magnetic beads (Dynabeads Protein G, Life Technologies) after 3h incubation at 4°C. The immunoprecipitated DNA fragments were eluted from the beads after 30 min incubation at 37°C in 10 mM DTT containing TE buffer, diluted 1:100 and followed by a second immunoprecipitation using anti-AhR (Enzo BML-SA210) or control rabbit IgG antibody, at 4°C. The AhR bound DNA fragments were collected through magnetic beads separation and chromatin was extracted and purified as described above. The relative enrichment of ChIP versus IgG (relative to input DNA) precipitated DNA was determined by qPCR analysis using the following primer pair: IL10 -8600: FW: 5'-AGGTCTATGAGCAGATTCATCCA-3', REV: 5'-CACCCTAGGGATGGTGTTGAT-3'.

Analysis of published ChIP-Seq data

ChIP-seq SRA datasets (11,12,13,14) of STAT3 (GSM1004860, GSM1004861), c-Maf (GSM1004799, GSM1004800), RORγt (GSM1004855, GSM1004856), Hif1-α (GSM1004819, GSM1004820), BATF (GSM1004786, GSM1004787), IRF4 (GSM1004827, GSM1004828, GSM1004831), p300 (GSM1004849, GSM1004850), histone modifications H3K27ac (GSM2905773, GSM2905774) and H3K4me1 (GSM2429057, GSM2429058) from *in vitro* differentiated Th17 cells were downloaded using the sra toolkit prefetch command, and converted to fastq files using fastq-dump. Fastq quality

control and preprocessing were performed as described above, while high quality reads were aligned to the UCSC mm9 reference genome using bwa-mem (15) using default settings and allowing 2 mismatches between the subject and the reference sequences. Alignments were further filtered as described above and UCSC genome browser tracks were generated using bedtools (16) and UCSC tools (17). Peaks were called using MACS2 suite, and any called peak with fold change less than 1 and FDR value over 0.01 was filtered out.

In silico regulatory region analyses of selected genes

The analyses aimed at the identification of the consensus binding sequences of AhR, c-Maf and STAT3 in the mouse *Nt5e* and *Entpd1* genes. Gene sequences for *Nt5e* and *Entpd1* with the accession numbers ENSMUSG00000032420 and ENSMUSG00000048120, respectively, were extracted from the Ensembl database (http://www.ensembl.org/index.html). The retrieved regulatory regions extending 5000bp upstream to 5000bp downstream of every known TSS of each gene were submitted to the MatInspector platform in Genomatix Database (http://www.genomatix.de/en/index.html) to identify putative TF binding sites (TBFS) for all the TF of Matrix Family Library Version 9.0, which contains 1381 weight matrices. In order to filter the output of the algorithm, the experimentally-verified TFBS of the known regulators in *Nt5e* and *Entpd1* (10,11) were considered as evidence of true positive results. Any predicted TFBS with *p* values and scores beyond the values of the experimentally-verified ones were excluded from the results.

In silico structural Study of AhR-ARNT-STAT3 interactions

STAT3 and AhR-ARNT were requested from the Protein Data Bank (PDB) (www. rcsb.org/pdb/home/home.do) and the most relevant solved structures (with PDB ID codes 3CWG and

5V0L, respectively) were retrieved. The solved structure of the heterodimeric Hif1-α-ARNT complex with HRE DNA (PDB ID code 4ZPR) was extracted as a reference structure for positive control docking experiments. The molecular docking experiments were performed via the pyDockweb server (18). The calculations of the binding affinities (ΔG) and dissociation constant (Kd) values of the complexes were performed with PRODIGY (PROtein binDIng enerGY prediction) (19). The molecular dynamics simulations were performed at Gromacs forcefield for 10ns with the help of MDWEB (20). Superimpositions, rmsd calculations and visualization of the structures were performed using the PyMOL Package (DeLano, W.L. The PyMOL Molecular Graphics System 2002 DeLano Scientific, San Carlos, CA, USA. http://www.pymol.org).

RNA Sequencing and bioinformatics analyses

RNA-sequencing libraries were generated for Th17 or act-A-Th17 cells using the Illumina's TruSeq RNA Library Preparation Kit v2 (Illumina, Inc.) and the sequencing was implemented with HiSeq 2000 by the European Molecular Biology Laboratory (EMBL). First, quality control of raw FastQ read files was performed using fastQC (Babraham Bioinformatics) and when appropriate, adapter contaminants were clipped and low quality sequenced bases were trimmed (Phred score > 10) using cutadapt (21), allowing a minimum of 20 bases/read. Consequently, high-quality reads were aligned to the University of California Santa Cruz (UCSC) mm9 reference genome using tophat2 (22) with parameters: *--library-type fr-unstranded --keep-fasta-order --bowtie1 --read-mismatches 2*. The alignments were further filtered for a mapping quality score of 10, using samtools (23), and only alignments on canonical chromosomes were kept using bash programming. Finally, differential expression analysis was performed using the Bioconductor package metaseqR (24). Alignment counts were summarized on Ensembl exons and were normalized for RNA composition effects using the trimmed mean of M-values

method by edgeR (24). Genes with (i) length < 500bp and (ii) average read counts per 100bp < 0.25 quantile of the average normalized read count distribution per 100bp in the gene body, were excluded to avoid possible statistical artifacts. DESeq was used for differential expression analysis providing results with log2 (FC) ≥ 1. The 972 identified DEGs were further processed using the Ingenuity Pathway Analysis tool to identify potential canonical pathway enrichment, upstream regulator effects and disease and downstream functional associations.

Quantitative proteomics analyses

Proteomics analysis. Cell pellets were dissolved in 0.5 M triethylammonium bicarbonate (TEAB), 0.05% sodium dodecyl sulphate (SDS) and subjected to pulsed probe sonication (Misonix, Farmingdale, NY, USA). Cell lysates were then centrifuged (16,000 g, 10 min, 4^{o}C) and supernatants were measured for protein content using the BCA protein assay kit (Thermo Fisher Scientific, Waltham, MA, US). A total of 100 μg of protein was used per sample, adjusted to the highest volume. Proteins were reduced [tris 2-carboxyethyl phosphine hydrochloride (TCEP), 4 μL of 50mM solution, incubation at 60^{o}C for 1 hour], alkylated [methyl-methanethiosulfonate (MMTS), 2 μL of 200mM solution, incubation at room temperature for 15 min) and enzymatically proteolyzed using trypsin (1:25). Peptides from each sample were labelled using twelve of the TMTpro reagents (Thermo Fisher Scientific, Waltham, MA, US). Labelled peptides were mixed and analysed using two-dimensional liquid chromatography and tandem mass spectrometry as reported previously (25). The labelling scheme was as follows: The six control Th17 cell specimens were labelled with the reagents TMTpro-126, TMTpro-127N, TMTpro-127C, TMTpro-128N, TMTpro-128C, and TMTpro-129N; the six Act-A treated Th17 cell specimens were labelled with the reagents TMTpro-129C, TMTpro-130N, TMTpro-130C, TMTpro-131N, TMTpro-131C, and TMTpro-132N. The quenched peptide samples were combined then initially fractionated

followed by offline Ultra-High Performance Liquid Chromatography with a RP C_4 stationary phase chemistry (Kromasil 150 × 2.1 mm, 3.5 µm particle, 100 Å pore size, Merck KGaA, Darmstadt, Germany) using gradient mobile phase conditions under alkaline conditions, as previously reported (25). Fractionated peptides were orthogonally concatenated, then dried down and stored at −80 °C until mass spectrometry analysis. Liquid chromatography-mass spectrometry (LC-MS) analysis was carried out on an EASY-nLC 1000 (ThermoFisher Scientific, San Jose, CA) coupled to an Orbitrap Eclipse Tribrid mass spectrometer (Thermo Fisher Scientific, San Jose, CA). Peptides samples were resuspended in 2% ACN, 0.2% formic acid, and 3-4ug peptides per concatenated sample were loaded onto an UHPLC monolithic column (Capillary EX-Nano MonoCap C18 HighResolution 2000, 0.1 x 2000 mm, Merck, Darmstadt Germany) fitted with a silica coated PicoTip emitter (New Objective FS360-20-10-D) and separated over 180 min at a flow rate of 0.5 µL/min with the following gradient: 2–6% Solvent B (10 min), 6-40% B (135 min), 40-100% B (1 min), and 100% B (34 min). Solvent A consisted of 97.8% H_2O, 2% ACN, and 0.2% formic acid, and solvent B consisted of 19.8% H_2O, 80% ACN, and 0.2% formic acid.

AGNOSTIC DISCOVERY STAGE: MS1 spectra were acquired in the Orbitrap at 120K resolution with a scan range from 375-2000 m/z, an AGC target of 4e5, and a maximum injection rate of 50 ms in Profile mode. Features were filtered for monoisotopic peaks with a charge state of 2-7 and a minimum intensity of 2.5e4, with dynamic exclusion set to exclude features after 1 time for 60 seconds with a 5-ppm mass tolerance. HCD fragmentation was performed with collision energy of 32% after quadrupole isolation of features using an isolation window of 0.7 m/z, an AGC target of 5e4, and a maximum injection time of 86 ms. MS2 scans were then acquired in the Orbitrap at 50K resolution in Centroid mode with the first mass fixed at 110. Cycle time was set at 1 second (**Figure M1**).

Proteomics data analysis was performed in Proteome Discoverer 2.4 (Thermo Scientific) using the Byonic search algorithm (Protein Metrics) and Uniprot mouse database (August 2018 download). Byonic search parameters were as follows: fully Tryptic peptides with no more than 2 missed cleavages, precursor mass tolerance of 10 ppm and fragment mass tolerance of 20 ppm (Orbi-MS2 runs) or 0.5 Da (Ion Trap MS2 scans in RTS-MS3 method), and a maximum of 3 common modifications and 2 rare modifications. Static modifications were cysteine carbamidomethylation and TMTpro addition to lysines and peptide N-termini. Methionine oxidation and lysine acetylation were common dynamic modifications (up to 2 each). Methionine loss on protein N-termini, methionine loss + acetylation on protein N-termini, protein N-terminal acetylation, and phosphorylation of serine, threonine, and tyrosine were rare dynamic modifications (only 1 each). Percolator FDRs were set at 0.001 (strict) and 0.01 (relaxed). Spectrum file retention time calibration was used with TMTpro addition to peptide N-termini and lysines as static modifications. Reporter ion quantification used a co-isolation threshold of 20, average reporter S/N threshold of 10, and SPS mass match threshold of 75%. Normalization was performed on total peptide amount and scaling was performed on all average. Peptide and protein FDRs were set at 0.001 (strict) and 0.01 (relaxed), with peptide confidence at least medium, lower confidence peptides excluded, and minimum peptide length set at 6. A one-sample T-Test with the Benjamini, Krieger and Yekutieli step-up method for multiple testing corrections was performed. Proteins identified with at least two unique peptides, with a mean TMT $\log_2$ratio higher than ± 0.58 (1.5-fold change) and a one-sample T-Test $q<0.05$, were considered differentially expressed.

GNOSTIC VERIFICATION STAGE: To verify the accuracy of relative quantitation of key biologically relevant proteins from the Discovery stage, the RTS-MS3 runs were performed as follows: MS1 spectra were acquired in the Orbitrap at 120K resolution with a scan range from 375-2000 m/z, an AGC target of 1e6, and a maximum injection rate of 50 ms in Profile mode. Features were filtered for monoisotopic

peaks with a charge state of 2-7 and a minimum intensity of 1e4, with dynamic exclusion set to exclude features after 1 time for 60 seconds with a 10 ppm mass tolerance. CID fragmentation was performed with collision energy of 35%, activation time of 10 ms, and activation Q of 0.25 following quadrupole isolation of features using an isolation window of 0.4 m/z, an AGC target of 1e4, and a maximum injection time of 45 ms. MS2 scans were then acquired in the Ion Trap using Rapid scan rate in Centroid mode. Real-time search parameters were set for fully Tryptic peptides with a maximum of 1 missed cleavage and up to two variable modifications. Static modifications were cysteine carbamidomethylation and TMTpro addition to lysines and peptide N-termini. Variable modifications were methionine oxidation and serine, threonine, and tyrosine phosphorylation. Scoring thresholds were Xcorr = 1, dCn = 0, precursor mass error of 10 ppm, and charge state not 1. Maximum search time was set to 35 ms. Up to 20 MS2 features matching identified peptide b- and y- ions were selected by SPS after filtering for mass range of 300-2000 m/z, TMTpro tag addition, and a precursor ion exclusion window between -50 m/z and +5 m/z. HCD fragmentation of SPS ions was performed with a fixed collision energy of 55%. MS3 quadrupole isolation used an isolation window of 0.7, an AGC target of 2.5e5, and a maximum injection time of 118 ms. MS3 spectra were then acquired in the Orbitrap at 60K resolution in Centroid mode with a scan range of 100-500 m/z. Cycle time was set for 3 seconds (**Figure M1**).

Proteomics data analysis was performed in Proteome Discoverer 2.4 (Thermo Scientific) using the Bionic search algorithm (Protein Metrics) and Uniprot mouse database (August 2018 download). Bionic search parameters were as follows: fully Tryptic peptides with no more than 2 missed cleavages, precursor mass tolerance of 10 ppm and fragment mass tolerance of 20 ppm (Orbi-MS2 runs) or 0.5 Da (Ion Trap MS2 scans in RTS-MS3 method), and a maximum of 3 common modifications and 2 rare modifications. TMTpro addition to lysine and peptide N-termini were static modifications. Methionine oxidation and lysine acetylation were common dynamic modifications (up to 2 each). Methionine loss

on protein N-termini, methionine loss + acetylation on protein N-termini, protein N-terminal acetylation, and phosphorylation of serine, threonine, and tyrosine were rare dynamic modifications (only 1 each). Percolator FDRs were set at 0.001 (strict) and 0.01 (relaxed). Spectrum file retention time calibration was used with TMTpro addition to peptide N-termini and lysines as static modifications. Reporter ion quantification used a co-isolation threshold of 20, average reporter S/N threshold of 10, and SPS mass match threshold of 75%. Normalization was performed on total peptide amount and scaling was performed on all average. Peptide and protein FDRs were set at 0.001 (strict) and 0.01 (relaxed), with peptide confidence at least medium, lower confidence peptides excluded, and minimum peptide length set at 6 (**Figure M1**).

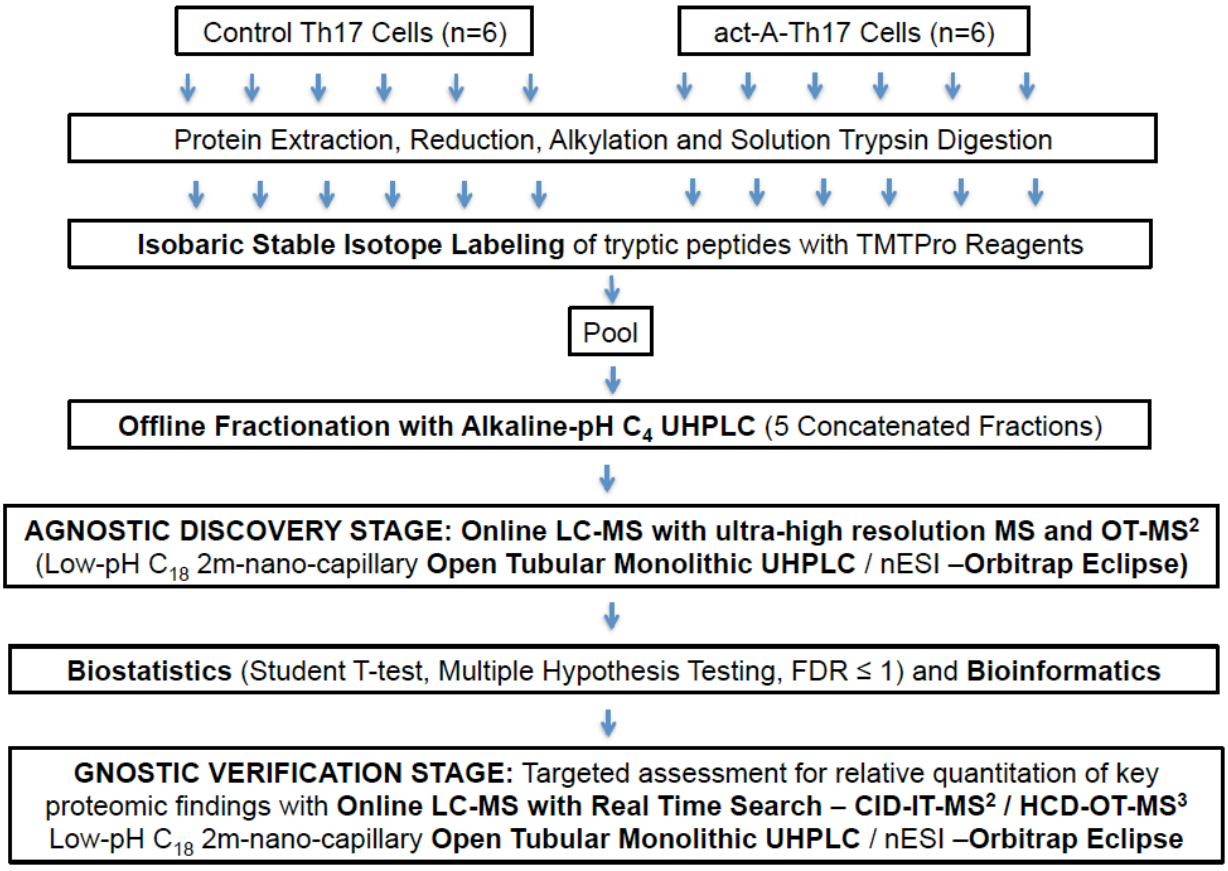

Figure M1. Two-stage Quantitative Proteomics Experimental Workflow

Proteomics data processing and biostatistics

Unprocessed raw files were submitted to Proteome Discoverer 2.3 for target decoy search using Byonic. The UniProtKB mus musculus database (release date January 2020) was utilized. The search allowed for up to two missed cleavages, a precursor mass tolerance of 10ppm, a minimum peptide length of six and a maximum of two variable (one equal) modifications of; oxidation (M), deamidation (N, Q), or phosphorylation (S, T, Y). Methylthio (C) and TMTpro (K, N-terminus) were set as fixed modifications. FDR corrected p-value at the peptide level was set at <0.01. Percent co-isolation excluding peptides from quantitation was set at 50. The TMT ratios of proteins were median-normalized and log2t. We considered the ratio of Activin-A treated cells vs. control cells per mouse and then log2transformed them. A one-sample T-Test with the Benjamini, Krieger and Yekutieli step-up method for multiple testing correction was performed. Proteins identified with a one-sample T-Test q<0.05, were considered differentially expressed in act-A-Th17 cells vs control-treated Th17 cells. IPA was used to identify significantly enriched canonical pathways, protein interaction networks and upstream regulators. DAVID (https://david.ncifcrf.gov/) was used to identify significantly over-represented GO terms. The threshold of significance was set at p-value ≤ 0.05.

Data availability

The RNA-Seq datasets generated in the current study have been deposited to the Gene Expression Omnibus (GEO) database and are assigned with the accession number GSE146439 (https://www.ncbi.nlm.nih.gov/geo/query/acc.cgi?acc=GSE146439). The mass spectrometry proteomics data have been deposited to the ProteomeXchange Consortium via the PRIDE partner repository with the dataset identifier PXD017757 (http://www.ebi.ac.uk/pride/archive/projects/PXD017757).

Statistical analysis

The number of independent experiments, biological replicates and donors analyzed are stated in each figure legend. Graph Pad Prism Version 6 (Graph Pad Software Inc.) was used for all statistical analyses. All data are presented as mean ± SEM. To calculate differences between groups, we used Student's t test, one-way and two-way ANOVA for repeated measures with post hoc Bonferroni correction, the Mann-Whitney test and the Wilcoxon matched-pairs signed rank test as appropriate. We considered any difference with a p value of 0.05 or less to be statistically significant ($*p \leq 0.05$, $**p \leq 0.01$ and $***p \leq 0.001$).

SI Figures and Figure Legends

Figure S1

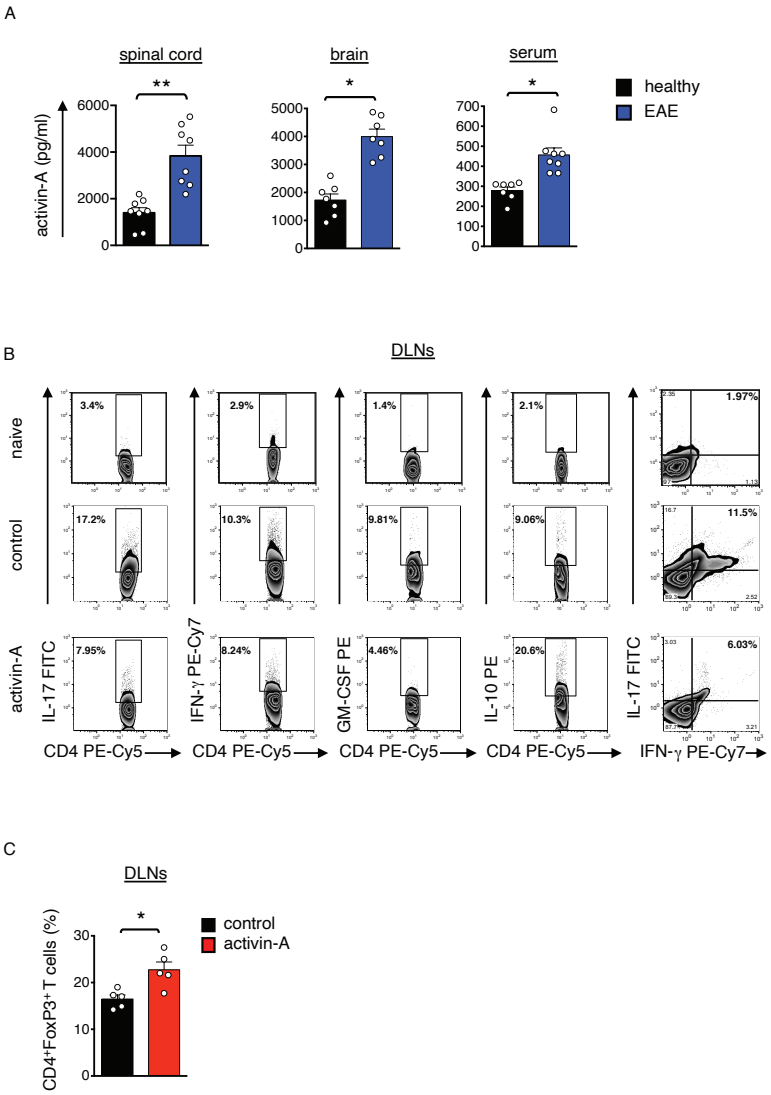

Figure S1. *In vivo* administration of activin-A attenuates EAE and restrains T effector responses. (**A**) Activin-A levels in the spinal cord, brain and serum of healthy mice and mice with EAE. Each symbol represents the mean±SEM of triplicate wells and corresponds to an individual mouse (*n*=7-8 mice/group). Data are representative of two independent *in vivo* experiments. (**B**) Representative FACS plots showing cytokine-expressing DLN T cells in an *ex vivo* MOG_{35-55} recall assay from mice

administered with activin-A or control (PBS), as in Fig. 1*B*. Cytokine-producing DLN T cells from nonimmune mice are also displayed. Data are representative of three independent experiments (*n*=6 mice/group). (**C**) Cumulative data showing the percentages of $CD4^+Foxp3^+$ T cells in the DLNs of mice treated with activin-A or control (PBS). Each symbol corresponds to an individual mouse (*n*=5 mice/group). Statistical significance was obtained by Student's t test; $*p < 0.05$, $**p < 0.01$.

Figure S2

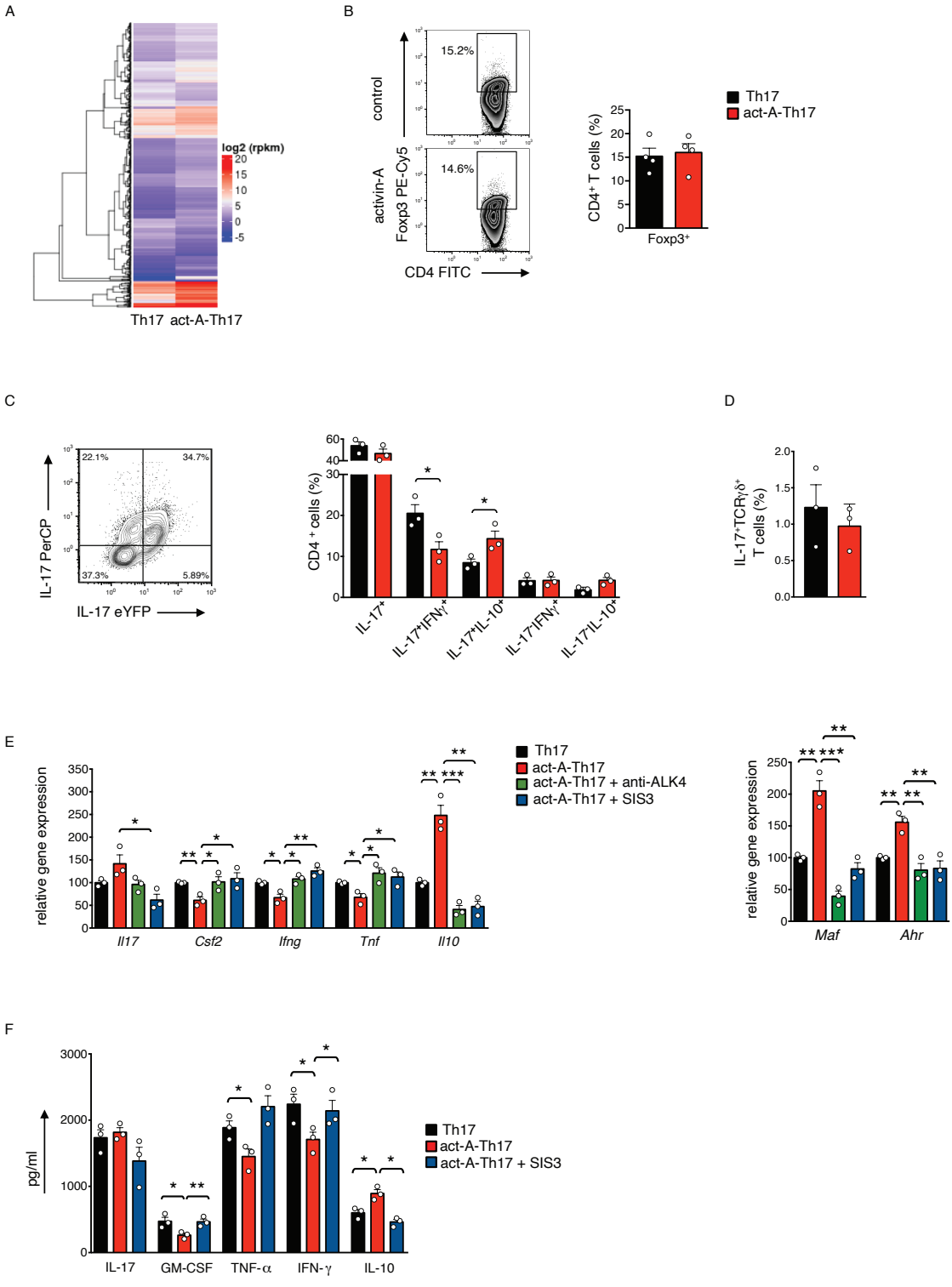

Figure S2. Activin-A represses the pathogenic signature of Th17 cells.

(**A**) Th17 or act-A-Th17 cells were generated as in Fig. 2. Heatmap and hierarchical clustering of gene expression (logarithmized rpkm values) depicting the transcriptional profile of 972 DEGs (log2 (FC) ≥ 1) in act-A-Th17 cells, relative to Th17 cells. (**B**) Representative FACS plots (left panels) and cumulative data (right panel) showing Foxp3 expression, gated on $CD4^+$ T cells. Data are mean±SEM and each symbol represents an independent *in vitro* experiment (*n*=4). (**C**) Th17 or act-A-Th17 cells were generated from *Il17a*^{Cre}*R26R*^{eYFP} reporter mice, as in Fig. 2. Representative FACS plot (left) and cumulative data (right) depicting cytokine-producing $CD4^+$ T cells and (**D**) IL-$17^+\gamma\delta^+$ T cells. Each symbol represents an independent *in vitro* experiment (*n*=3). (**E**) Th17 or act-A-Th17 cells were generated as indicated. Gene expression was analyzed by qPCR and normalized to *Gapdh* and *Polr2a*. Each symbol represents the mean±SEM of duplicate wells and corresponds to a separate *in vitro* experiment (*n*=3). (**F**) Cytokine release in culture supernatants of Th17 or act-A-Th17 cells, generated as in Fig. 2. Each symbol represents the mean±SEM of triplicate wells and corresponds to a separate *in vitro* experiment (*n*=3). Statistical analysis was performed by unpaired Student's t test; **p* < 0.05, ***p* < 0.01 and ****p* < 0.001.

Figure S3

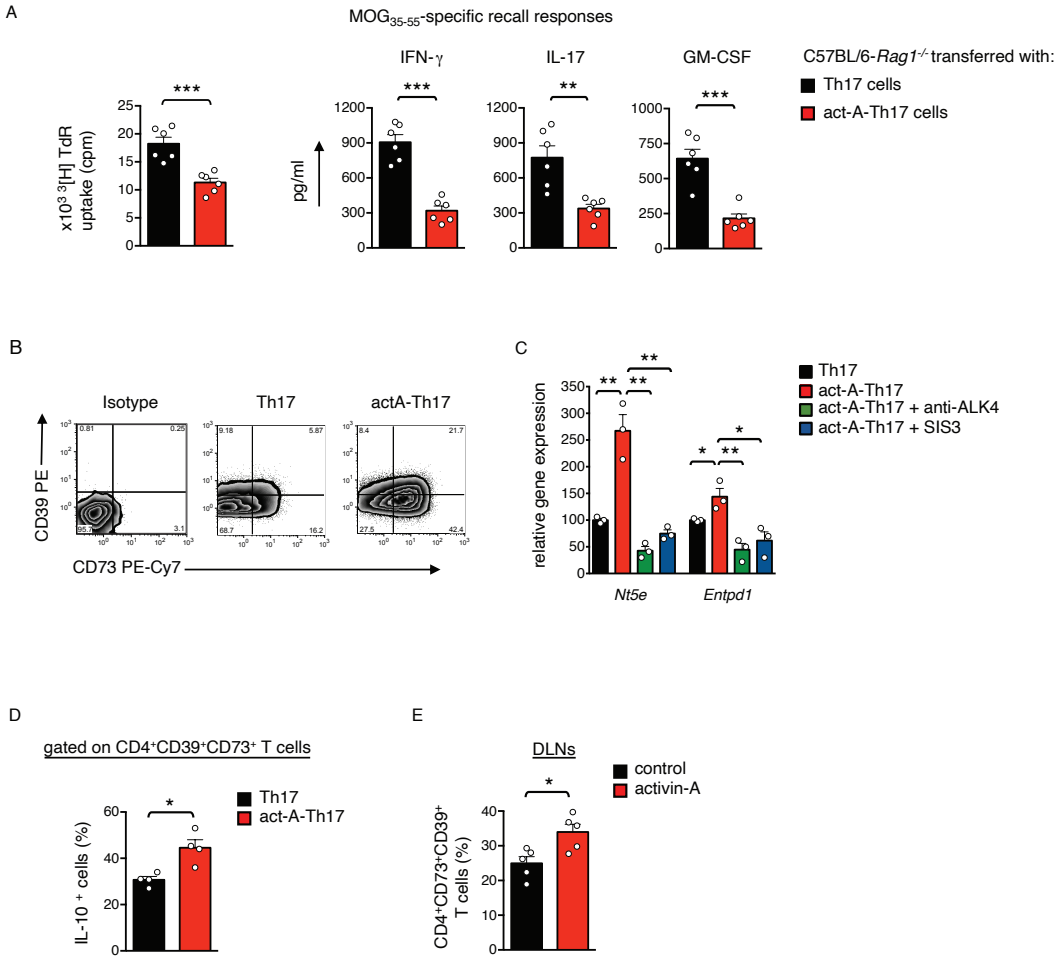

Figure S3. Activin-A suppresses the encephalitogenic potential of Th17 cells.

(**A**) T cell proliferation and cytokine release by DLN cells from C57BL/6-*Rag1*$^{-/-}$ recipients, restimulated with MOG_{35-55} *ex vivo*. Each symbol represents the mean±SEM of triplicate wells and corresponds to an individual mouse (*n*=6 mice/group). (**B**) Th17 or act-A-Th17 cells were generated as in Fig. 2. FACS plots showing CD39 and CD73 expression, gated on $CD4^+$ T cells. Data are representative of *n*=4 independent *in vitro* experiments. Isotype controls are also shown. (**C**) Gene expression was analyzed by qPCR and normalized to *Gapdh* and *Polr2a*. Each symbol represents the

mean±SEM of duplicate wells and corresponds to a separate *in vitro* experiment (*n*=3). (**D**) Cumulative data showing the percentages of IL-10^{+}CD39^{+}CD73^{+}CD4^{+} T cells. Data are mean±SEM and each symbol represents a separate *in vitro* experiment (*n*=4). (**E**) Cumulative data showing the percentages of CD73^{+}CD39^{+}CD4^{+} T cells among DLN cells, generated as in Fig. 1, from control or activin-A -treated mice. Each symbol corresponds to an individual mouse (*n*=5 mice/group). Statistical analysis was performed by unpaired Student's t test; *$p < 0.05$, **$p < 0.01$ and ***$p < 0.001$.

Figure S4

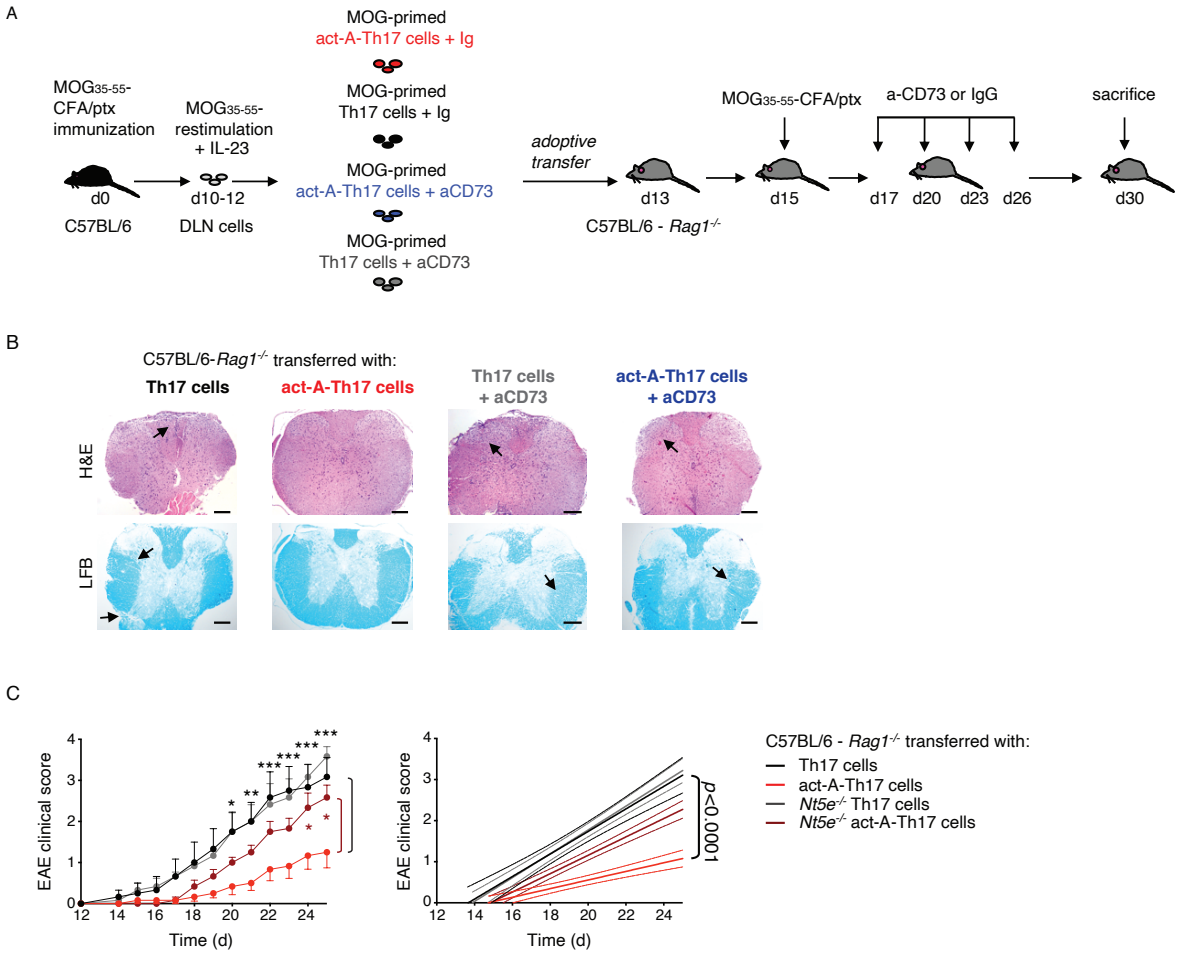

Figure S4. Blockade of CD73 signaling reverses activin-A-induced suppression of Th17 cell encephalitogenicity.

(**A**) Experimental protocol utilized. (**B**) H&E and LFB stainings on spinal cord sections in C57BL/6-*Rag1*$^{-/-}$ mice transferred with act-A-Th17 cells or Th17 cells (bars, 50μm). Data are representative of two independent experiments (n=5 mice/group). (**C**) Clinical scores of C57BL/6-*Rag1*$^{-/-}$ mice reconstituted with act-A-Th17 cells or Th17 cells, obtained from CFA/MOG-immunized *Nt5e*$^{+/+}$ or *Nt5e*$^{-/-}$ mice. Linear regression analysis of the clinical scores is depicted on the right. Statistical significance was obtained by two-way ANOVA, followed by Bonferroni's multiple comparisons test.

Results are mean±SEM and represent one out of two independent experiments (n=6 mice/group); *p < 0.05, **p < 0.01 and ***p < 0.001.

Figure S5

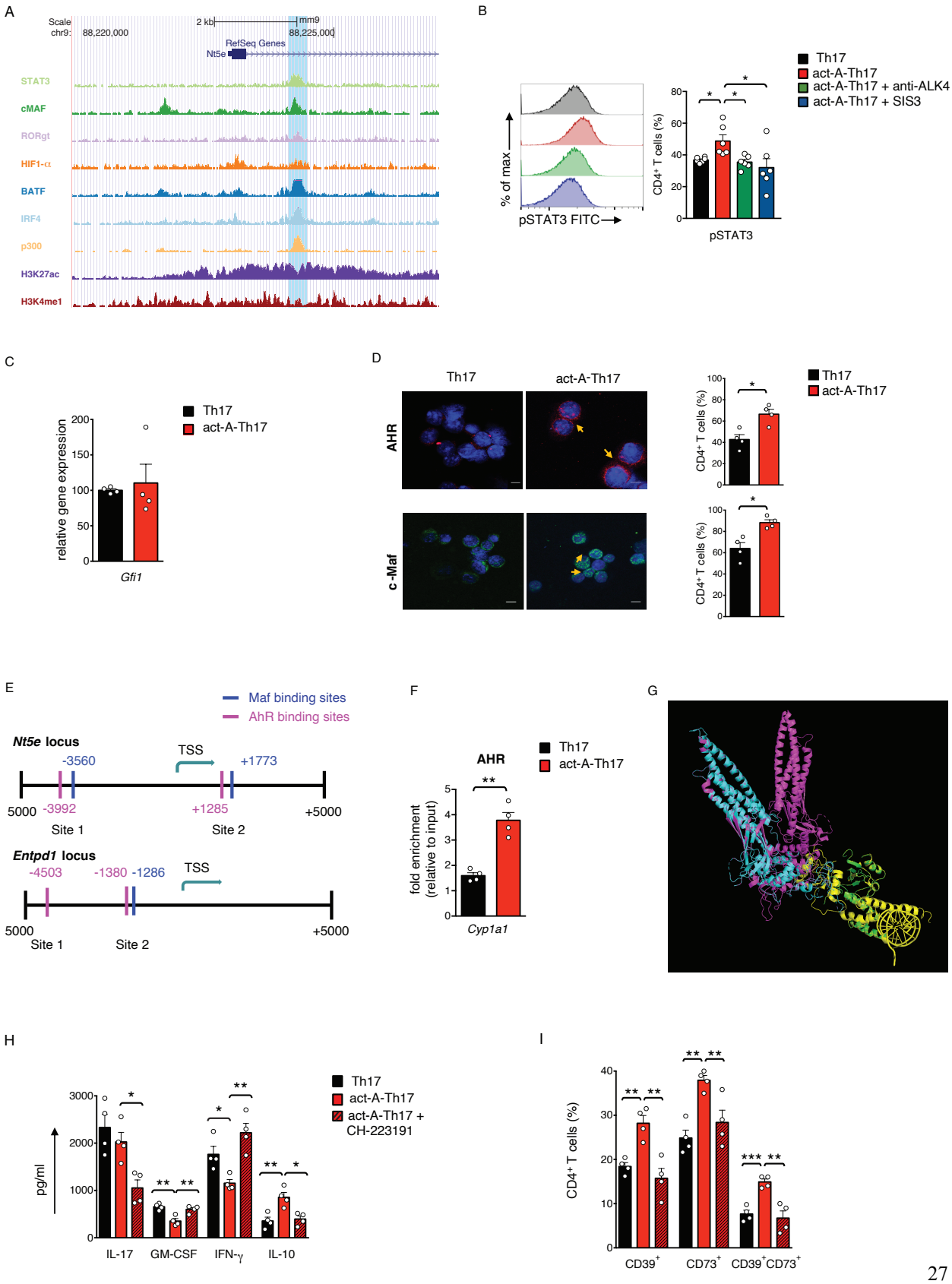
A
Scale
chr9:
88,220,000
2 kb
mm9
88,225,000
RefSeq Genes
Nt5e
STAT3
cMAF
RORgt
HIF1-α
BATF
IRF4
p300
H3K27ac
H3K4me1
B
% of max
pSTAT3 FITC
CD4+ T cells (%)
pSTAT3
Th17
act-A-Th17
act-A-Th17 + anti-ALK4
act-A-Th17 + SIS3
C
relative gene expression
Gfi1
Th17
act-A-Th17
D
Th17
act-A-Th17
AHR
c-Maf
CD4+ T cells (%)
E
Maf binding sites
AhR binding sites
Nt5e locus
-3560
TSS
+1773
5000
-3992
+1285
+5000
Site 1
Site 2
Entpd1 locus
-4503
-1380
-1286
TSS
5000
+5000
Site 1
Site 2
F
AHR
fold enrichment (relative to input)
Cyp1a1
Th17
act-A-Th17
G
H
pg/ml
IL-17
GM-CSF
IFN-γ
IL-10
Th17
act-A-Th17
act-A-Th17 + CH-223191
I
CD4+ T cells (%)
CD39+
CD73+
CD39+CD73+

Figure S5. AhR and c-Maf drive activin-A-induced CD73 upregulation in Th17 cells.

(**A**) University of California, Santa Cruz genome browser snapshot of the extended Nt5e genomic region around the TSS. In the highlighted region, 1,700 bp downstream the TSS, colocalization of TFs and H3K27ac and H3K4me1 signals are detected. (**B**) Act-A-Th17 or Th17 cells were generated as in Fig. 2. Representative FACS plots showing pSTAT3 expression, gated on $CD4^+$ T cells. Grey histogram represents isotype control. Cumulative data are shown as mean±SEM. Each symbol represents a separate *in vitro* experiment (*n*=6). (**C**) Th17 or act-A-Th17 cells were generated as in Fig. 2. Gene expression was analyzed by qPCR and normalized to *Gapdh* and *Polr2a*. Each symbol represents the mean±SEM of duplicate wells and corresponds to a distinct *in vitro* experiment (*n*=4). (**D**) Representative confocal microscopy images (left panels) and cumulative data (right panels) of $CD4^+$ T cells stained with anti-AhR (red) or anti-c-Maf (green) antibodies, as indicated. Nuclei are stained blue with DAPI (bars, 20μm). Data are mean±SEM and each symbol represents a separate *in vitro* experiment (*n*=4). (**E**) Schematic representation of the mouse *Nt5e* and *Entpd1* loci showing the putative AhR and c-Maf binding sites. (**F**) ChIP analysis demonstrating the binding of AhR on the *Cyp1a1* promoter. Data are mean±SEM and each symbol represents a separate *in vitro* experiment (*n*=4). (**G**) Computational model of the putative protein-protein interactions of STA3 and AhR is shown. Superimpositions of the solved structures of AhR/ARNT in complex with the DRE [PDB code:5V0L] (yellow) and the unphosphorylated mouse STAT3 core fragment [PDB code:3CWG] (magenta), comprising the docked pose of AhR-ARNT complex (green) with STAT3 (cyan). The DNA is shown in yellow. (**H**) Act-A-Th17 or Th17 cells were generated as in Fig. 2. Cytokine release in culture supernatants is shown. Each symbol represents the mean±SEM of triplicate wells and corresponds to a separate *in vitro* experiment (*n*=4). (**I**) The percentages of CD39 and CD73 -expressing $CD4^+$ T cells are shown. Data are mean±SEM and each symbol represents a separate *in*

vitro experiment (n=4). Statistical analysis was performed by unpaired Student's t test; *$p < 0.05$, **$p < 0.01$ and ***$p < 0.001$.

Figure S6

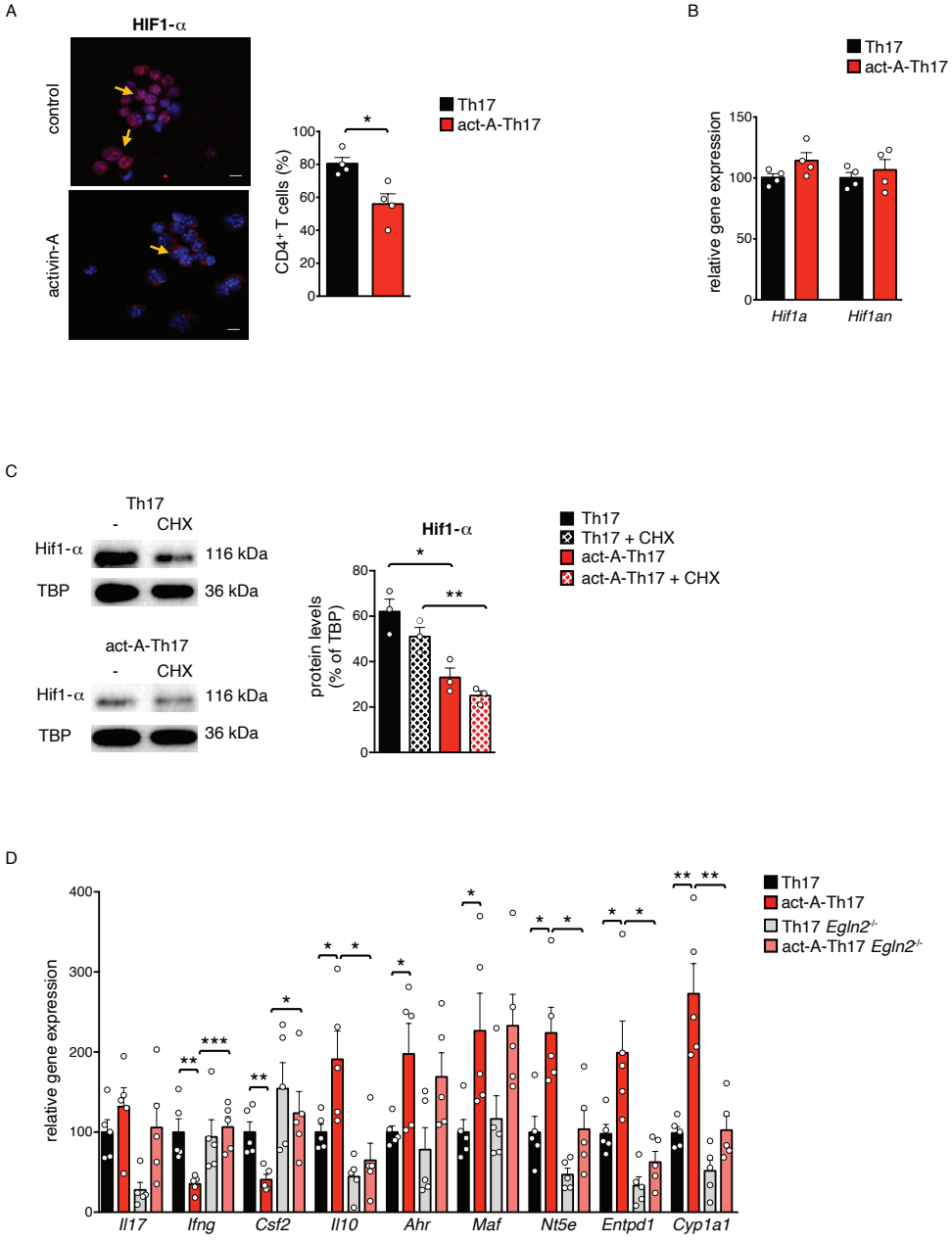

Figure S6. Activin-A affects Hif1-α stability in Th17 cells.

(**A**) Representative confocal microscopy images (left panels) and cumulative data (right panel) of Th17 or act-A-Th17 cells stained with fluorescently-conjugated anti-Hif1-α antibody (red). Nuclei are stained blue with DAPI (bars, 20μm). Data are mean±SEM and each symbol represents a separate *in*

vitro experiment (*n*=4). (**B**) Th17 or act-A-Th17 cells were generated, as in Fig. 2. Gene expression was analyzed by qPCR and normalized to *Gapdh* and *Polr2a*. Each symbol represents the mean±SEM of duplicate wells and corresponds to a distinct *in vitro* experiment (*n*=4). (**C**) Representative immunoblots showing Hif1-α expression in control- and cycloheximide-treated (CHX) Th17 or act-A-Th17 cells, as indicated. Quantification of relative Hif1-α protein levels are depicted on the right; TATA Binding protein (TBP). Data are mean±SEM and each symbol represents a separate *in vitro* experiment (*n*=3). (**D**) Naive $CD4^+$ T cells were isolated from the spleen and lymph nodes of C57BL/6 mice or *Egln2*$^{-/-}$ mice, and differentiated under Th17-polarizing conditions (as in Fig. 2). Gene expression was analyzed by qPCR and normalized to *Gapdh* and *Polr2a*. Each symbol represents the mean±SEM of duplicate wells and corresponds to a distinct experiment (*n*=5). Statistical analysis was performed by unpaired Student's t test; $*p < 0.05$, $**p < 0.01$ and $***p < 0.001$.

Figure S7

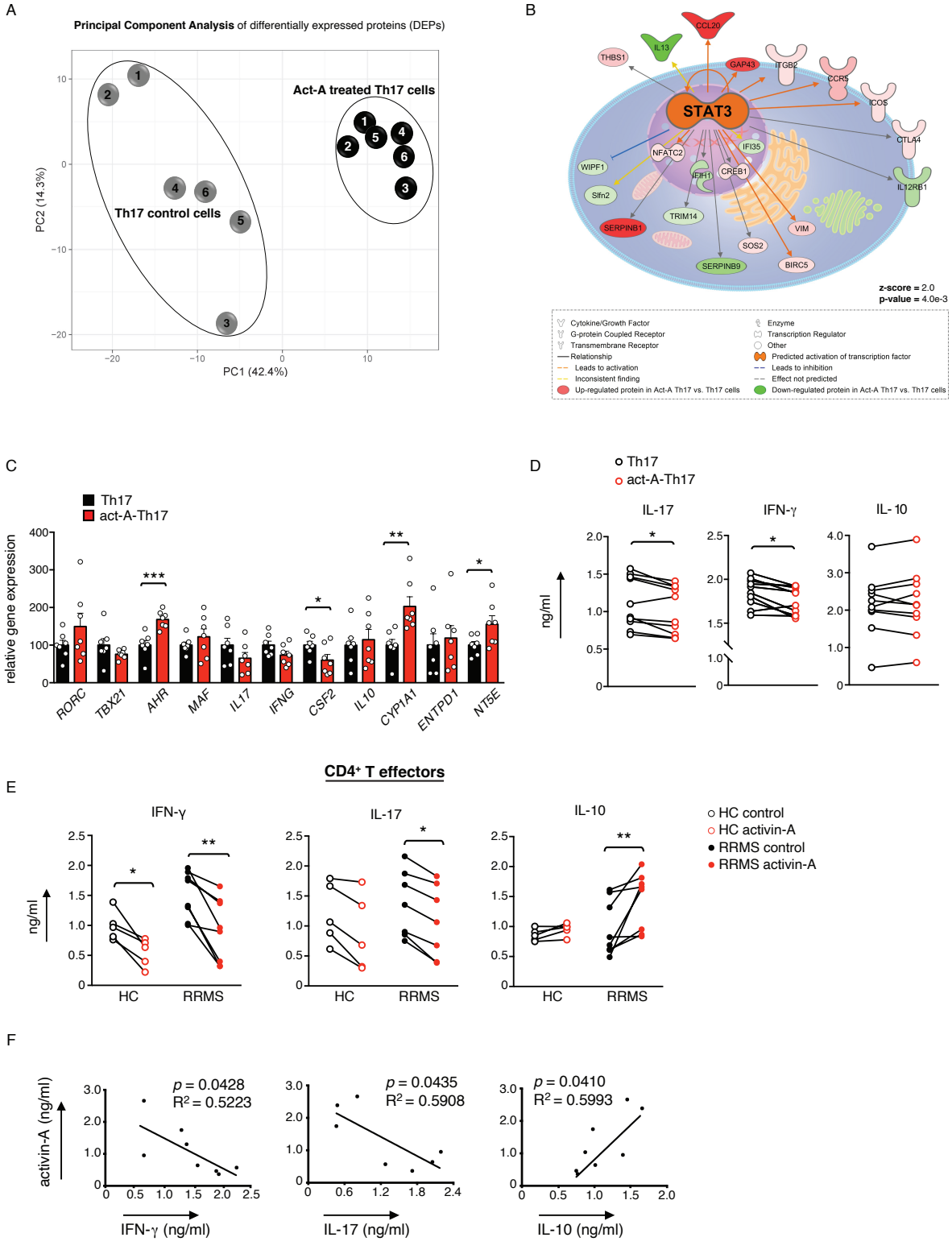
A
Principal Component Analysis of differentially expressed proteins (DEPs)
Act-A treated Th17 cells
Th17 control cells
PC1 (42.4%)
PC2 (14.3%)
B
CCL20
IL13
THBS1
GAP43
ITGB2
CCR5
ICOS
STAT3
CTLA4
IFI35
NFATC2
WIPF1
IFIH1
CREB1
IL12RB1
Sifn2
TRIM14
SERPINB1
VIM
SOS2
SERPINB9
BIRC5
z-score = 2.0
p-value = 4.0e-3
Cytokine/Growth Factor
G-protein Coupled Receptor
Transmembrane Receptor
Relationship
Leads to activation
Inconsistent finding
Up-regulated protein in Act-A Th17 vs. Th17 cells
Enzyme
Transcription Regulator
Other
Predicted activation of transcription factor
Leads to inhibition
Effect not predicted
Down-regulated protein in Act-A Th17 vs. Th17 cells
C
Th17
act-A-Th17
relative gene expression
RORC
TBX21
AHR
MAF
IL17
IFNG
CSF2
IL10
CYP1A1
ENTPD1
NT5E
D
Th17
act-A-Th17
IL-17
IFN-γ
IL-10
ng/ml
E
CD4+ T effectors
IFN-γ
IL-17
IL-10
ng/ml
HC
RRMS
HC control
HC activin-A
RRMS control
RRMS activin-A
F
activin-A (ng/ml)
p = 0.0428
R2 = 0.5223
IFN-γ (ng/ml)
p = 0.0435
R2 = 0.5908
IL-17 (ng/ml)
p = 0.0410
R2 = 0.5993
IL-10 (ng/ml)

Figure S7. Activin-A restrains pro-inflammatory CD4$^+$ T effector T responses in RRMS patients. (**A**) Principal Component Analysis of DEPs showed that act-A-Th17 cells clustered separately from control-treated Th17 cells. (**B**) IPA predicted that STAT3 is significantly activated based on downstream analyzed proteins in act-A-Th17 cells. (**C**) Naive CD4$^+$ T cells from healthy controls were polarized towards the Th17 cell lineage, in the presence or absence of activin-A. Gene expression was analyzed by qPCR and normalized to *B2M*. Data are mean±SEM of duplicate wells; each symbol depicts an individual donor (n=7). Statistical significance was obtained by the Mann-Whitney test; *p < 0.05 and **p < 0.01. (**D**) Cytokine release was quantitated in culture supernatants. Each symbol represents the mean±SEM of triplicate wells and corresponds to an individual donor (n=10). Statistical significance was obtained by the Wilcoxon matched-pairs signed rank test. (**E**) CD4$^+$ T cells, isolated from the peripheral blood of RRMS patients and healthy donors (HC), were stimulated with antibodies against CD3/CD28 and activin-A or PBS (control). Cytokine release in culture supernatants is shown. Data are mean±SEM of triplicate wells; each symbol depicts an individual donor (n=5-7). Statistical significance was obtained by the Wilcoxon matched-pairs signed rank test; *p < 0.05 and **p < 0.01. (**F**) Correlation of activin-A expression in the serum with IL-10, IL-17 and IFN-γ levels in the supernatants of peripheral blood CD4$^+$ T cells from RRMS patients, stimulated as above. Linear regression analysis was performed.

Figure S8

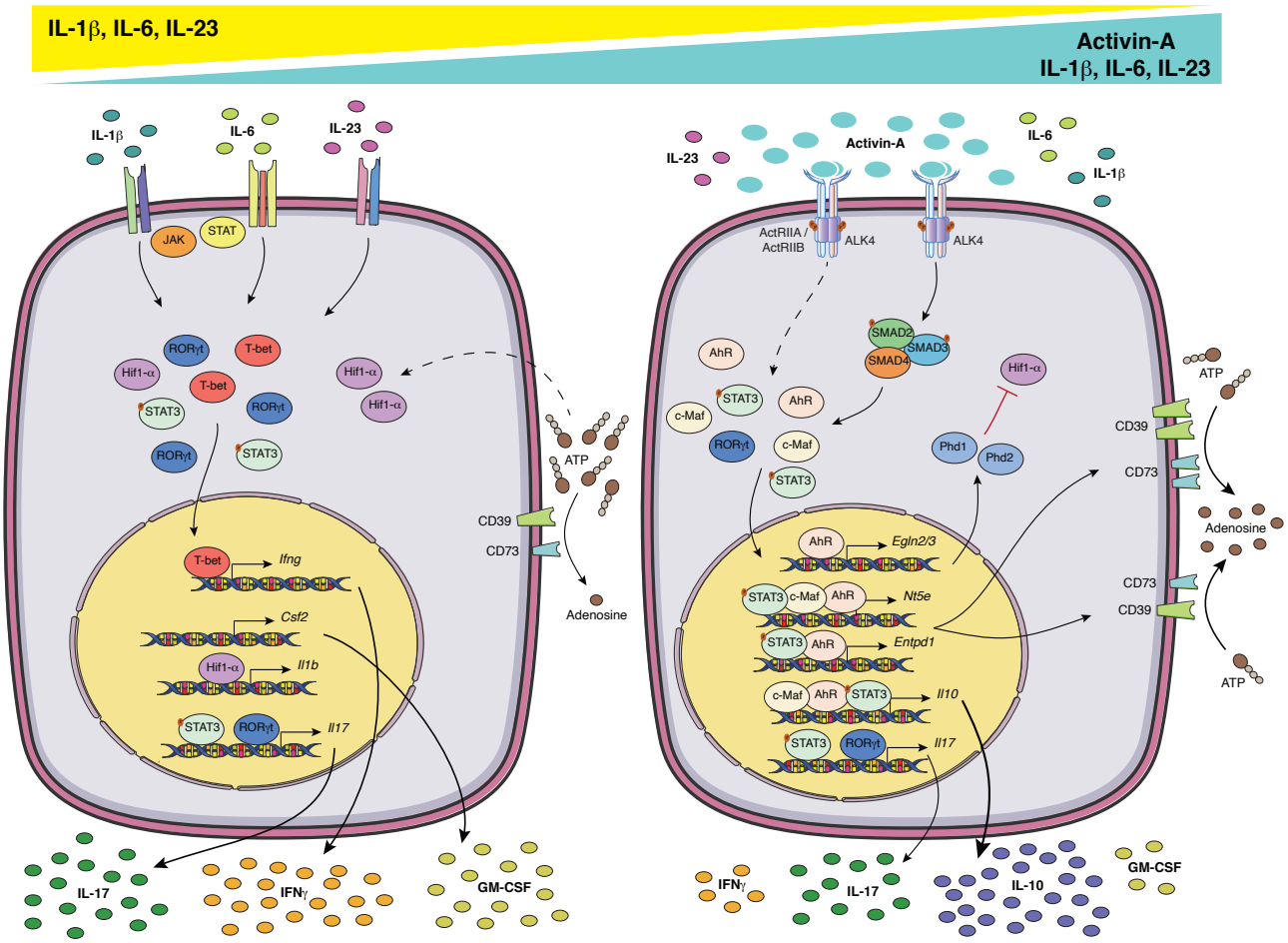

Figure S8. Activin-A represses the pathogenic signature of Th17 cells.

Schematic representation of the proposed molecular mechanisms through which activin-A restrains the pathogenic Th17 cell signature. Activin-A binds to its type I and type II receptors which activate its canonical pSmad2/3 intracellular pathways. These, in turn, induce AhR, STAT3 and c-Maf activation which enter the nucleus and direct CD39, CD73 and IL-10 upregulation in Th17 cells. Concomitantly, AhR drives Phd1 protein expression which, along with Phd2, decrease Hif1-α stability. CD39 and CD73 localize at the Th17 cell surface wherein they deplete eATP and further dampen Hif1-α

signaling. Altogether, these activin-A-triggered molecular events lead to enhanced IL-10 production and decreased IFN-γ and GM-CSF release and render Th17 cells less pathogenic.

Table S1. Clinical characteristics of the study population.

	Healthy Controls	Disease Controls	RRMS[A] Patients
n	10	20	23
Age (years, mean ± SD)	48.7 ± 7.7	44.2 ± 11.5	52.5 ± 10.1
Female : Male (*n*)	6:4	12:8	16:7
Disease (*n*)			
Multiple Sclerosis	-	-	23
Viral encephalitis	-	8	-
TB meningitis	-	4	-
Diplopia	-	8	-
MS disease duration[B]	-	-	
(median, range)			10 (2-19)
EDSS (median, range)	-	-	2 (0,5-6)
Treatment (*n*)			
Natalizumab	-	-	7
Interferon	-	-	6
Fingolimod	-	-	5
Glatiramer acetate	-	-	4
Dimethyl fumarate	-	-	1

[A]RRMS = relapsing remmiting multiple sclerosis,

[B]Disease duration = years

Table S2. Primer pairs used for the real-time PCR analyses.

Gene	Species	Forward primer	Reverse primer
Il17a	*M. Musculus*	TCATCCCTCAAAGCTCAGCG	TTCATTGCGGTGGAGAGTCC
Tnf		CCAGACCCTCACACTCACAA	ATAGCAAATCGGCTGACGGT
Ifng		GCGTCATTGAATCACACCTG	TGAGCTCATTGAATGCTTGG
Il1b		ACCTTCCAGGATGAGGACATGA	CTAATGGGAACGTCACACACCA
Csf2		CTCACCCATCACTGTCACCC	TGAAATTGCCCCGTAGACCC
Il10		TGAATTCCCTGGGTGAGAAG	GCTCCACTGCCTTGCTCTTA
Rorc		CCCGAGATGCTGTCAAGTTT	CTTGGCCACTTGTTCCTGTT
Tbx21		GGTGTCTGGGAAGCTGAGAG	GAAGGACAGGAATGGGAACA
Maf		CCCTTGACAGTTTGCTTCTA	CCCATTCTGCTATCTTTGAC
Ahr		CTCCTTCTTGCAAATCCTGC	GGCCAAGAGCTTCTTTGATG
Foxp3		CCCATCCCCAGGAGTCTTG	ACCATGACTAGGGGCACTGTA
Cyp1a1		TCAGTCCCTCCTTACAGCCC	GGGTTCTTCCCCACAGTCAG
Nt5e		CTACCCAGGAACTCGGGAGA	GGATGCCACCTCCGTTTACA
Entpd1		GGAAACCTGATCTGTGATGC	CTTCAGGGTGGACCCTTTTA
Gzmb		GACCAAACGTGCTTCCTTTC	GCAGGATCCATGTTGCTTCT
Lag3		ACATTCAACCAGACAGTGGCCA	GCATCCCCTGGTGAAGGTC
Egln1		AGGCTATGTCCGTCACGTTG	TGGGCTTTGCCTTCTGGAAA
Egln2		GTAGAAGGTCACGAGCCAGG	CGCCATGCACCTTAACATCC
Egln3		AGGCAATGGTGGCTTGCTAT	GACCCCTCCGTGTAACTTGG
Hif1a		AGTGCTGATCCTGCACTGAA	AGGCTGGGAAAAGTTAGGAGTG
Hif1an		CCGTGGGGAGGAAGATTGTC	CACTCGAACTGATCCGGAGG
Gfi1		TCAAATGCAGCAAGGTGTTC	ACAGTCAAAGCTGCGTTCCT
Glut1		CACTGTGGTGTCGCTGTTTG	AAAGATGGCCACGATGCTCA
Pdhk1		ACGGGACAGATGCGGTTATC	GCTTCCAGGCGGCTTTATTG
Ldha		GCATGGCAGCCTCTTCCTTA	GTTTCGCTGGACCAGGTTGA
Uqcrh		CATGGGACTAGAGGACGAACG	AGCTGTTCACAGTGCTCTCTC
B2M	*H. Sapiens*	TGAGTATGCCTGCCGTGTGA	TGATGCTGCTTACATGTCTCGAT
RORC		GCAGCGCTCCAACATCTTCTC	GCACACCGTTCCCACATCTC
TBX21		GATGCGCCAGGAAGTTTCAT	GCACAATCATCTGGGTCACATT

AHR		CCGTGTCGATGTATCAGTGC	GCCTGGCAGTACTGGATTGT
MAF		ACGAGAAGTTGGTGAGCAGC	TTCCAAAATGTGGCGTATCC
IL17A		AAGAACTTCCCCCGGACTGT	GTGGTAGTCCACGTTCCCAT
IFNG		TTGGAAAGAGGAGAGTGACAGAA	TGCGTTGGACATTCAAGTCAG
IL10		GGCGCTGTCATCGATTTCTT	TTGGAGCTTATTAAAGGCATTCTTC
CSF2		CCTGGGAGCATGTGAATGCCA	GGTCGGCTCCTGGAGGTCAA
NT5E		CTGGGAGAACCTGGCTGCTG	CACATGGATTCCGCCCACCT
ENTPD1		GGATGCGGGTTCTTCTCACA	CCCAGGTAAACGGGTGTCTC
CYP1A1		CAGCTGACTTCATCCCTATTC	AGCTGGACATTGGCGTTCTCA

SI References

1. C. Teunissen, T. Menge, A. Altintas, J.C. Álvarez-Cermeño, A. Bertolotto, F.S. Berven, L. Brundin, M. Comabella, M. Degn, F. Deisenhammer, F. Fazekas, D. Franciotta, J.L. Frederiksen, D. Galimberti, S. Gnanapavan, H. Hegen, B. Hemmer, R. Hintzen, S. Hughes, E. Iacobaeus, A.C. Kroksveen, J. Kuhle, J. Richert, H. Tumani, L.M. Villar, J. Drulovic, I. Dujmovic, M. Khalil, A. Bartos, Consensus definitions and application guidelines for control groups in cerebrospinal fluid biomarker studies in multiple sclerosis. *Mult Scler*. **13**, 1802–1809 (2013)
2. E.V. Dang, J. Barbi, H.Y. Yang, D. Jinasena, H. Yu, Y. Zheng, Z. Bordman, J. Fu, Y. Kim, H.-R. Yen, W. Luo, K. Zeller, L. Shimoda, S.L. Topalian, G.L. Semenza, C.V. Dang, D.M. Pardoll, and F. Pan, Control of TH17/Treg Balance by Hypoxia-Inducible Factor 1. *Cell*. **146**, 772–784 (2011)
3. J. Aragonés, M. Schneider, K. Van Geyte, P. Fraisl, T. Dresselaers, M. Mazzone, R. Dirkx, S. Zacchigna, H. Lemieux, N.H. Jeoung, D. Lambrechts, T. Bishop, P. Lafuste, A. Diez-Juan, S.K. Harten, P. Van Noten, K. De Bock, C. Willam, M. Tjwa, A. Grosfeld, R. Navet, L. Moons, T. Vandendriessche, C. Deroose, B. Wijeyekoon, J. Nuyts, B. Jordan, R. Silasi-Mansat, F. Lupu, M. Dewerchin, C. Pugh, P. Salmon, L. Mortelmans, B. Gallez, F. Gorus, J. Buyse, F. Sluse, R.A. Harris, E. Gnaiger, P. Hespel, P. Van Hecke, F. Schuit, P. Van Veldhoven, P. Ratcliffe, M. Baes, P. Maxwell and P. Carmeliet. Deficiency or inhibition of oxygen sensor Phd1 induces hypoxia tolerance by reprogramming basal metabolism. *Nat. Genet.* **40**, 170–180 (2008)
4. A.L. Croxford, F.C. Kurschus, and A. Waisman, Cutting Edge: An IL-17F-CreEYFP Reporter Mouse Allows Fate Mapping of Th17 Cells. *J Immunol*. **182**, 1237–1241 (2019)
5. S. Srinivas, T. Watanabe, C.-S. Lin, C.M. William, Y. Tanabe, T.M. Jessell, and F. Costantini, Cre reporter strains produced by targeted insertion of EYFP and ECFP into the ROSA26 locus. *BMC Dev Biol*. **1**, 4 (2001)
6. S. Tousa, M. Semitekolou, I. Morianos, A. Banos, A.I. Trochoutsou, T.M. Brodie, N. Poulos, K. Samitas, M. Kapasa, D. Konstantopoulos, G. Paraskevopoulos, M. Gaga, C.M. Hawrylowicz, F. Sallusto, and G. Xanthou, Activin-A co-opts IRF4 and AhR signaling to induce human regulatory T cells that restrain asthmatic responses. *Proc Natl Acad Sci U S A*. **114**, E2891-E2900 (2017)
7. I.M. Stromnes, and J.M. Goverman, Active induction of experimental allergic encephalomyelitis. *Nat Protoc*. **1**, 1810–1819 (2006)

8. M. Semitekolou, T. Alissafi, M. Aggelakopoulou, E. Kourepini, H.H. Kariyawasam, A.B. Kay, D.S. Robinson, C.M. Lloyd, V. Panoutsakopoulou, and G. Xanthou, Activin-A induces regulatory T cells that suppress T helper cell immune responses and protect from allergic airway disease. *J Exp Med*. **206**, 1769–1785 (2009)
9. K.J. Livak, and T.D. Schmittgen, Analysis of Relative Gene Expression Data Using Real-Time Quantitative PCR and the 2−ΔΔCT Method. *Methods*. **25**, 402–408 (2001)
10. I.D. Mascanfroni, M.C. Takenaka, A. Yeste, B. Patel, Y. Wu, J.E. Kenison, S. Siddiqui, A.S. Basso, L.E. Otterbein, D.M. Pardoll, F. Pan, A. Priel, C.B. Clish, S.C. Robson, and F.J. Quintana, Metabolic control of type 1 regulatory T cell differentiation by AHR and HIF1-α. *Nat Med*. **21**,638–646 (2015)
11. M. Ciofani, A. Madar, C. Galan, M. Sellars, K. Mace, F. Pauli, A. Agarwal, W. Huang, C.N. Parkurst, M. Muratet, K.M. Newberry, S. Meadows, A. Greenfield, Y. Yang, P. Jain, F.K. Kirigin, C. Birchmeier, E.F. Wagner, K.M. Murphy, R.M. Myers, R. Bonneau, and D.R. Littman, A Validated Regulatory Network for Th17 Cell Specification. *Cell*. **151**, 289–303 (2012)
12. F. Chalmin, G. Mignot, M. Bruchard, A. Chevriaux, F. Végran, A. Hichami, S. Ladoire, V. Derangère, J. Vincent, D. Masson, S.C. Robson, G. Eberl, J.R. Pallandre, C. Borg, B. Ryffel, L. Apetoh, C. Rébé, and F. Ghiringhelli, Stat3 and Gfi-1 Transcription Factors Control Th17 Cell Immunosuppressive Activity via the Regulation of Ectonucleotidase Expression. *Immunity*. **36**, 362–373 (2012)
13. Y. Jiang, Y. Liu, H. Lu, S.-C. Sun, W. Jin, X. Wang, and C. Dong, Epigenetic activation during T helper 17 cell differentiation is mediated by Tripartite motif containing 28. *Nat Commun*. **9**, 1424 (2018)
14. X.-P. Yang, K. Ghoreschi, S.M. Steward-Tharp, J. Rodriguez-Canales, J. Zhu, J.R. Grainger, K. Hirahara, H.-W. Sun, L. Wei, G. Vahedi, Y. Kanno, J.J. Oshea, and A. Laurence, Opposing regulation of the locus encoding IL-17 through direct, reciprocal actions of STAT3 and STAT5. *Nat Immunol*. **12**, 247–254 (2011)
15. L. Heng, Aligning sequence reads, clone sequences and assembly contigs with BWA-MEM. Available at https://arxiv.org/abs/1303.3997. V2. Deposited 16 Mar 2013
16. A.R. Quinlan, and I.M. Hall, BEDTools: a flexible suite of utilities for comparing genomic features. *Bioinformatics*. **26**, 841–842 (2010)

17. W.J. Kent, A.S. Zweig, G. Barber, A.S. Hinrichs, and D. Karolchik, BigWig and BigBed: enabling browsing of large distributed datasets. *Bioinformatics*. **26**, 2204–2207 (2010)
18. B. Jimenez-Garcia, C. Pons and J. Fernandez-Recio. "pyDockWEB: a web server for rigid-body protein-protein docking using electrostatics and desolvation scoring". *Bioinformatics*. **29**, 1698-1699 (2013)
19. Xue L., Rodrigues J., Kastritis P., Bonvin A.M.J.J.*, Vangone A.*, "PRODIGY: a web-server for predicting the binding affinity in protein-protein complexes". *Bioinformatics.* **32**, 3676-3678 (2016)
20. Adam Hospital, Pau Andrio, Carles Fenollosa, Damjan Cicin-Sain, Modesto Orozco, Josep Lluís Gelpí. MDWeb and MDMoby: an integrated web-based platform for molecular dynamics simulations. *Bioinformatics*. **28**, 1278-1279 (2012)
21. M. Martin, Cutadapt removes adapter sequences from high-throughput sequencing reads. *EMBnet*. **17**, 10 (2011)
22. D. Kim, G. Pertea, C. Trapnell, H. Pimentel, R. Kelley, and S.L. Salzberg, TopHat2: accurate alignment of transcriptomes in the presence of insertions, deletions and gene fusions. *Genome* Biol. 14, R36 (2013)
23. H. Li, B. Handsaker, A. Wysoker, T. Fennell, J. Ruan, N. Homer, G. Marth, G. Abecasis, and R. Durbin, The Sequence Alignment/Map format and SAMtools. *Bioinformatics*. **25**, 2078–2079 (2009)
24. P. Moulos, and P. Hatzis, Systematic integration of RNA-Seq statistical algorithms for accurate detection of differential gene expression patterns. *Nucleic Acids Res*. **43,** e25 (2014)
25. A. Manousopoulou, A. Hayden, M. Mellone, D.J. Garay-Baquero, C.H. White, F. Noble, M. Lopez, G.J. Thomas, T.J. Underwood, and S.D. Garbis, Quantitative proteomic profiling of primary cancer-associated fibroblasts in oesophageal adenocarcinoma. *Br. J. Cancer*. **118**, 1200–1207 (2018)
26. B.K. Erickson, J. Mintseris, D.K. Scweppe, J. Navarrete-Perea, A.R. Erickson, D.P. Nusinow, J.A. Paulo and S.P. Gygi. Active Instrument Engagement Combined with a Real-Time Database Search for Improved Performance of Sample Multiplexing Workflows. *J Proteome Res.* **18**, 1299-1306 (2019)